Met Office
Hadley Centre

Hadley Centre Technical Note 98

Meridional overturning circulations driven by surface wind and buoyancy forcing

April 2015

Michael J. Bell

If printing double sided you will need this blank page. If printing single sided, please delete this page.

Meridional overturning circulations driven by surface wind and buoyancy forcing

MICHAEL J. BELL,*

Met Office, Exeter, UK

ABSTRACT

The Meridional Overturning Circulation (MOC) can be considered to consist of a downwelling limb in the Northern Hemisphere (NH) and an upwelling limb in the Southern Hemisphere (SH) that are connected via western boundary currents. Steady-state analytical gyre-scale solutions of the planetary geostrophic equations are derived for a downwelling limb driven in the NH solely by surface heat loss. In these solutions the rates of the water mass transformations between layers driven by the surface heat loss determine the strength of the downwelling limb. Simple expressions are obtained for these transformation rates which depend on the most southerly latitudes where heat loss occurs and the depths of the isopycnals on the eastern boundary. Previously derived expressions for the water mass transformation rates in sub-polar gyres driven by the Ekman upwelling characteristic of the SH are also summarised. Explicit expressions for the MOC transport and the depths of isopycnals on the eastern boundary are then derived by equating the water mass transformations in the upwelling and downwelling limbs. The MOC obtained for a "single-basin" 2-layer model is shown to be generally consistent with that obtained by Gnanadesikan (1999). The model's energetics are derived and discussed and solutions for the MOC obtained in a "single-basin" 3-layer model are also derived. In a world ocean without a circumpolar channel in the SH it is suggested that the upwelling limb would feed downwelling limbs in both hemispheres. In a world with two basins in the northern hemisphere, if one of them has a strong halocline the model suggests that the MOC would be very weak in that basin.

1. Introduction

This Technical Report is an extended version of a paper (Bell 2015a) that has been submitted for peer review. It contains an additional section and appendix that were omitted from that paper and a longer discussion comparing the new results with those in previous papers.

The Meridional Overturning Circulation (MOC) in the Atlantic Ocean is part of a complex global circulation in which dense water formed by surface cooling in the North Atlantic flows in deep western boundary currents into the Southern Hemisphere (SH) before re-surfacing south of the Antarctic Circumpolar Current (ACC) in a region of surface warming (Marshall and Speer 2012). Despite intensive study there are still differing conceptual views of the dynamics and energetics of this "conveyor belt" circulation (Huang 2010, sec 5.4). One point that is clear is that, as explained in Wunsch and Ferrari (2004) and Vallis (2006, sec 15.2), consideration of the energy budget shows that it is very unlikely that a consistent dynamical model of the MOC could be developed that is driven solely by surface buoyancy fluxes.

Following Cox (1989), various modeling studies have shown that the wind stresses in the South Atlantic have an important influence on the Atlantic MOC. Toggweiler and Samuels (1995) emphasized the role of the zonal mean Ekman transport at the northern edge of the Drake passage. Building on ideas about the momentum balance in the circumpolar channel, as presented for example by Rintoul *et al* (2001), Gnanadesikan (1999), hereafter referred to as G99, proposed a simple model for the strength of the MOC in which the strength of the overturning transport in the Southern Ocean is determined by the northward Ekman transport in the channel and the net southward transport by the time-varying "eddies" at mid-depths. Gnanadesikan closed his model of the MOC transports by using scaling arguments relating the strength of the baroclinic western boundary current in the North Atlantic and the diabatic mixing at the base of the thermocline to the depth of the thermocline. In G99 the strength of the MOC is determined by a cubic equation for the depth of the thermocline at mid-latitudes and is proportional to the square of this depth.

The main aim of this paper is to derive expressions for the MOC based on the rates of water mass transformations obtained in solutions to the planetary geostrophic equations (PGEs) and to compare these expressions with those obtained in G99. The simplest physical configuration for

*Corresponding author address: Dr Mike Bell, Met Office, Fitzroy Rd, Exeter, EX1 3PB, United Kingdom.
E-mail: mike.bell@metoffice.gov.uk

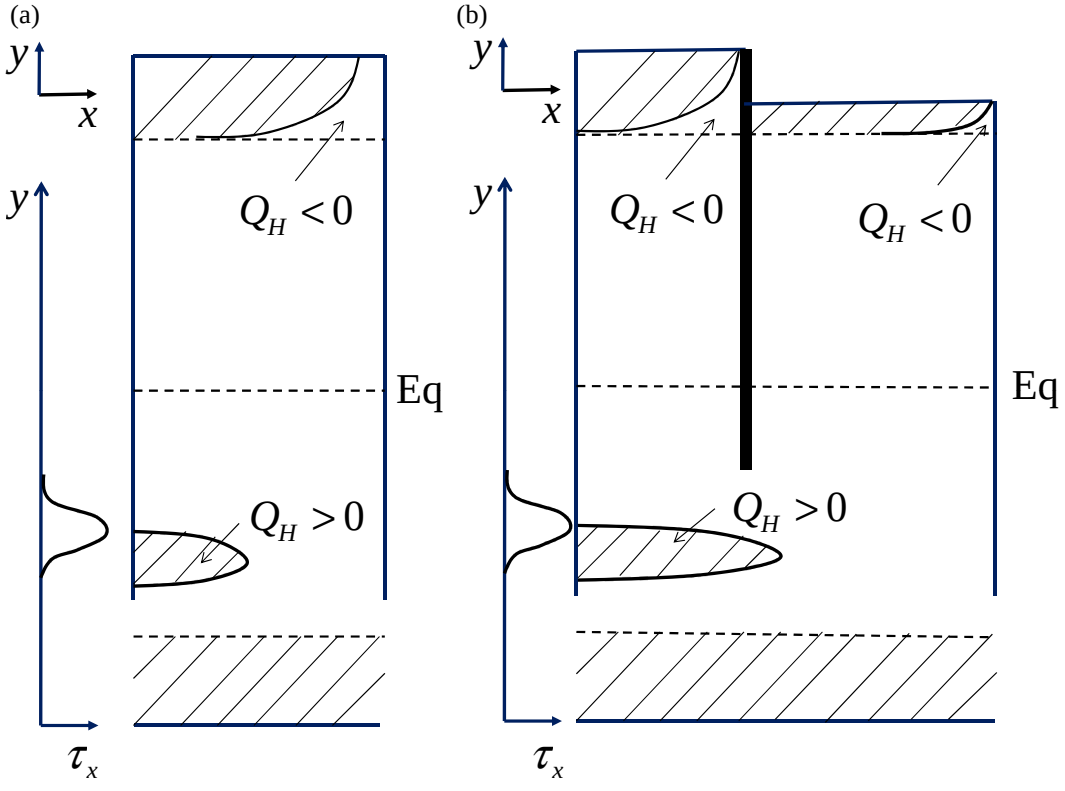

FIG. 1. (a) Depiction of the simplest ocean domain for which solutions are derived. The ocean occupies a rectangular basin spanning the equator with a periodic channel at its southern boundary. The model has only 2 isopycnal layers. The lower layer shoals or outcrops in the diagonally shaded regions. The surface heat flux into the ocean, Q_H, is only non-zero in the two regions shown. The zonal wind stress $\tau_x(y)$ is shown on the left of the figure. (b) The 2-basin configuration discussed in section 9b. The basins are separated by a "continent" which extends to about 30°S.

which solutions are obtained is illustrated in Figure 1a. Following many previous authors (e.g. Greatbatch and Lu 2003) the ocean domain is represented as a single basin which is closed in the Northern Hemisphere (NH) and has a periodic channel in the SH and the ocean itself is represented by a small number of isopycnal layers (only two layers in Figure 1a). Unlike many previous studies the strong surface westerlies in the SH are specified to be a maximum well to the north of the channel, as they are in re-analyses (Radko and Marshall 2006), and the basin is taken to span almost 360° of longitude. In order to simplify the calculations, the surface wind stress is taken to be zonal and to be zero in the latitudes of the channel. The atmospheric surface temperature is taken to vary with latitude being colder at high latitudes than at the equator.

The nature of the solutions that are obtained when the surface temperature varies only with latitude is indicated by the shaded regions in Figure 1a, which represent the regions in which the upper isopycnal layer either shoals or outcrops. The surface winds in the SH drive Ekman upwelling south of the wind stress maximum which causes the upper layer to shoal in the west of the basin. It is assumed that the surface atmosphere is warm enough at these latitudes for this to result in a positive surface heat flux into the ocean, $Q_H > 0$, which transforms water from the lower layer into water in the upper layer in this region of shoaling. The upper layer also outcrops in the south of the channel and the flow within the channel is purely zonal and in "thermal wind" balance with the sloping interface between the layers. The formulation of the buoyancy forcing used and the motivation for and derivation of these solutions for the SH have been presented in Bell (2015b), hereafter referred to as B15. These solutions with a sub-polar gyre to the north of Drake passage and an entirely separate zonal flow within the channel do not resemble the flow in the Southern Ocean very closely. But B15 suggests that if the wind stress field illustrated in figure 1 were moved southward the westward flow in the southern half of the gyre would also move south and "merge" with the eastward flow in the channel to leave a single circum-

polar flow which deflects sharply northward immediately to the east of Drake passage. The solutions capture the east-west asymmetry in the net surface heat fluxes at about $50-55^{\circ}$S which is prominent in a number of surface flux products (see Figure 5.2 of Josey *et al* 2013).

Along the eastern boundary of the ocean basin the boundary conditions used imply that the upper layer depth does not change with latitude. As a result at high latitudes in the NH, where the surface atmosphere is sufficiently cold, there is a region of substantial heat loss where water in the surface layer is transformed into water in the lower layer. Global steady state solutions are obtained by choosing the depth of the upper layer on the eastern boundary so that the heat lost from the upper layer at the surface in the NH is equal to the heat gained in the SH. It is assumed that northern and western boundary currents close the interior circulations. One can imagine that nearer the equator than the regions with non-zero Q_H discussed in this paper, additional warmer water layers overlie the two layers discussed here.

The rest of this paper is structured as follows. Section 2 briefly summarises the formulation of the model; B15 gives a more detailed discussion. Section 3 presents simple analytical calculations of the water mass transformations which occur at high latitudes when the model is driven in the NH solely by surface cooling. Section 4 briefly explains the conceptual summary of the results for water mass transformations driven by Ekman upwelling in the SH derived in B15. Section 5 presents a 2-layer model of the MOC obtained by combining the above solutions for the NH and SH. Section 6 compares the model's formulation and results with those of G99 and section 7 discusses the model's energetics.

Section 8 presents a 3-layer model of the MOC which was omitted from Bell (2015a) but may be of interest to mathematically-minded readers. The solutions and derivations are conceptually and qualitatively similar to those for the 2-layer model. In particular the depths of the two interfaces between the three layers on the eastern boundary are determined by the condition that the net surface heat flux into each layer should be zero and the total MOC transport is of similar magnitude to that of the 2-layer model. The technical details are however more complicated and it is recommended that this section be omitted on first reading. The appendix contains some mathematical details used in these derivations.

Section 9 discusses MOCs in a "world" without a circumpolar channel in the SH and in a world with two basins one of which has a strong halocline. Section 10 compares the models of the MOC and the Southern Ocean presented here with some previous models other than G99. This section spells out the main points more explicitly and covers a slightly wider range of papers than the corresponding discussion in the introduction of Bell (2015a). Section 11 summarises and discusses the simplifications used in the paper.

2. Governing equations

The PGEs will be taken to govern the motions in the ocean interior (i.e. outside "side-wall" boundary layers). These equations are appropriate for large-scale motions in the ocean with small Rossby number (see e.g. Vallis 2006, secs. 3.3 and 5.3). For simplicity they are written in Cartesian coordinates with x increasing eastward and y northward. Figure 2 illustrates the notation that will be used

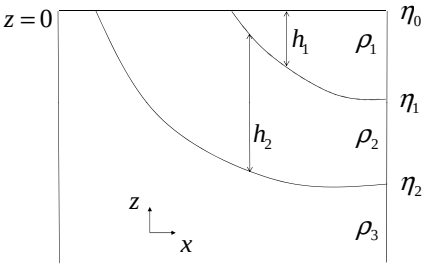

FIG. 2. Vertical section through a model with three layers. x and z are coordinates which increase eastward and with height respectively. $z=0$ at the ocean surface, h_i is the depth of the ith layer and η_i is the height of the interface at the base of the ith layer measured from $z=0$.

for the case of an ocean with three layers. h_i denotes the depth of the ith layer and η_i the height of the internal interface at the bottom of the ith layer measured from the constant geopotential surface $z=0$. The depth of the ocean bathymetry, $H(x,y)$, may vary in regions where the lowest layer is at rest (reduced gravity) but for simplicity will be taken to be flat in regions where the lowest layer is directly forced (either by buoyancy or wind forcing). The density, geopotential and horizontal velocities of the ith layer are denoted by ρ_i, ϕ_i and $\mathbf{u}_i=(u_i,v_i)$ respectively. Defining

$$\eta_0 = 0, \tag{1}$$

the layer depths and heights of the interfaces are related by

$$h_i = \eta_{i-1} - \eta_i, \quad 1 \le i \le N. \tag{2}$$

The planetary geostrophic approximations to the horizontal momentum, hydrostatic and continuity equations are then given by

$$f\hat{\mathbf{k}} \times \mathbf{u}_i = -\nabla\phi_i + \frac{\tau_i}{\rho_0 h_i}, \tag{3}$$

$$\phi_{i+1} = \phi_i + g_i\eta_i, \tag{4}$$

$$\frac{\partial h_i}{\partial t} + \nabla.(h_i \mathbf{u}_i) = Q_{i,i+1} - Q_{i-1,i}. \quad (5)$$

In (3) – (5), which will be taken to apply for $1 \le i \le N$, $f = 2\Omega \sin\varphi$ is the Coriolis parameter, where Ω is the Earth's rotation rate and φ is latitude, $\hat{\mathbf{k}}$ is the unit vector parallel to the z axis and $\tau_i = (\tau_{ix}, \tau_{iy})$ is the turbulent momentum flux absorbed in the ith layer (the wind stress on the layer if it is at the surface and sufficiently deep). In (5) $Q_{i,i+1}$ is the volume flux of water transformed from that of layer $i+1$ into that of layer i as a result of the surface buoyancy fluxes across the ocean surface and mixing processes. As in (1),

$$Q_{0,1} = 0. \quad (6)$$

The formulation of the parametrisation of $Q_{i,i+1}$ used here is discussed in detail in B15. The solutions derived in this paper have no freshwater fluxes and for this case

$$Q_{i,i+1} = \frac{\alpha_T Q_i^H}{c_P(\rho_{i+1} - \rho_i)}, \quad (7)$$

where Q_i^H is the net heat flux, α_T is the thermal expansion coefficient and c_P is the specific heat capacity of the water. When layer i is at the surface and the salinities in layers i and $i+1$ are the same, surface cooling Q_i^H will be parametrised by

$$Q_i^H = r_Q(T_A - T_i), \quad T_A < T_{i+1}, \quad (8)$$

in which $T_A(x,y)$ is an imposed atmospheric surface temperature, T_i is the temperature of the ith layer and r_Q is the Haney coefficient. This formulation requires the surface cooling to form water that is denser than that in the layer below the surface before convection occurs. Section 9b discusses a case in which the salinities of the two layers differ and (8) needs to be modified accordingly. Where the atmosphere surface temperature is warmer than that of the surface layer, the effective surface heating and the diabatic mixing are taken to reduce with the depth of the surface layer divided by a mixing length, λ_Q, and Q_i^H is specified by

$$Q_i^H = r_Q(T_A - T_i)\,\mathrm{e}^{\eta_i/\lambda_Q}, \quad T_A > T_i. \quad (9)$$

There is taken to be no heat flux for other surface temperatures

$$Q_i^H = 0, \quad T_{i+1} < T_A < T_i. \quad (10)$$

A model with only a small number of layers that uses (10), is likely to have zero values of $Q_{i,i+1}$ over quite wide regions of the domain. So the fluxes that are obtained using the above parametrisation in a two-layer model are of limited fidelity. This is one of the main motivations for the derivation of the N-layer surface cooling solution presented in subsection 3c. Together (8) and (10) result in a surface flux field that has discontinuities where the ith layer is at the surface along lines where $T_A = T_{i+1}$. For some purposes it certainly would be preferable to respecify (8) to avoid this but the solutions discussed in this paper are robust to such discontinuities.

This paper will only consider steady state solutions and will assume that the eastern boundary layers are unable to absorb any normal flow so that no-normal flow boundary conditions apply to all the layers. It also assumes that the wind stress parallel to the boundary is zero (as is the case when the winds are zonal and the boundaries lie due north-south). Denoting the eastern boundary by $x_E(y)$ and using (3) and (4) this implies that the geopotentials and the heights of the interfaces are constant along eastern boundaries

$$\phi_i(x_E(y), y) = \phi_i^0 \equiv \phi_{iE}, \quad (11)$$

$$\eta_i(x_E(y), y) = \eta_i^0 \equiv \eta_{iE}. \quad (12)$$

Northern and western boundary layers will be assumed to be able to absorb and re-circulate whatever flow is determined from the eastern boundary conditions and the interior equations (Huang and Flierl 1987).

The velocities $\mathbf{u}_i$ in (3) can be diagnosed from ϕ_i so (3) and (5) can be reduced to a single equation for each layer by multiplying (3) by h_i and substituting the resulting expression for $h_i\mathbf{u}_i$ into (5). Doing this and setting the time derivative in (5) to zero one obtains

$$J\left(\phi_i, \frac{h_i}{f}\right) = Q_{i,i+1} - Q_{i-1,i} - C_i, \quad 1 \le i \le N, \quad (13)$$

where J denotes the Jacobian derivative, which for any ϕ and ψ is given by

$$J(\phi,\psi) \equiv \frac{\partial\phi}{\partial x}\frac{\partial\psi}{\partial y} - \frac{\partial\phi}{\partial y}\frac{\partial\psi}{\partial x}, \quad (14)$$

and C_i is an expression for the Ekman pumping in the ith layer given by

$$\rho_0 C_i \equiv \nabla\times\left(\frac{\tau_i}{f}\right). \quad (15)$$

The total Ekman pumping, C, is calculated from the total wind stress, τ, as in (15).

The area integral of the rate of transformation of water from layer j to layer i, which is a volume flux with units $\mathrm{m}^3\mathrm{s}^{-1}$, will be denoted by

$$I_Q(i,j) \equiv \int\int Q_{i,j}\mathrm{d}x\mathrm{d}y. \quad (16)$$

These integrals for the NH and the SH are of primary importance because they describe/determine the MOC across the equator.

3. Water mass transformations driven in the NH solely by surface cooling

A particularly simple and informative set of analytical steady state solutions can be obtained when the surface

wind forcing is small enough in comparison to the surface heat loss to be ignored. This approximation can be made for a narrow basin, like the Atlantic, when $|Q_{1,2}| \gg |C|$ and hence C is negligible on the rhs of (13). The restriction to narrow basins is necessary because the wind field modifies the path of the characteristics in wide basins (see e.g. Schloesser *et al* 2014, or B15). In the North Atlantic, taking $\tau \approx 0.06\mathrm{Nm}^{-2}$ and $\Delta y \approx 2.10^6\mathrm{m}$ using (15) one finds that $|C| \approx 3\times10^{-7}\mathrm{m}^3\mathrm{s}^{-1}$. Using $T_1 = 10^\circ\mathrm{C}$ and $T_2 = 4^\circ\mathrm{C}$ one finds (e.g. using Gill 1982, appendix 3) that $\alpha_T \approx 1.310^{-4}\mathrm{K}^{-1}$, $c_P \approx 410^3\mathrm{Jkg}^{-1}\mathrm{K}^{-1}$ and $\rho_2 - \rho_1 \approx 0.83\mathrm{kgm}^{-3}$. Using these values in (7) gives $Q_{1,2} \approx 4\times10^{-8}Q_i^H$ where Q_1^H is expressed in Wm^{-2}. Since the net heat flux in the North Atlantic is of the order of $60\mathrm{Wm}^{-2}$ neglect of the surface wind stresses is reasonably well founded. T_A and Q_i^H will be allowed to vary with both longitude, x, and latitude, y, in this section.

a. Solutions in the layer at the surface next to the eastern boundary

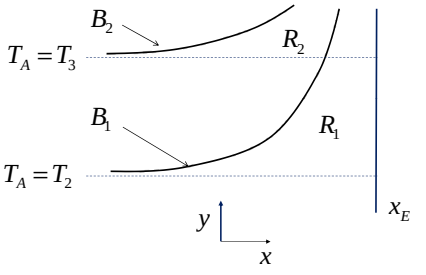

FIG. 3. Depiction of the regions R_i and boundaries B_i for the surface cooling calculation. Layer i outcrops along B_i. Region R_i is bounded to the west by B_i to the south by $T_A = T_{i+1}$ and to the east by $x = x_E$ when $i = 1$ and by B_{i-1} when $i > 1$

Consider first the solution for region R_1 which is illustrated and defined in Figure 3 and its caption. As only the two upper layers are directly forced, the lower layers can be taken to be at rest and hence

$$\phi_3 = \phi_{3E} = 0, \tag{17}$$

the constant value of ϕ_{3E} being taken to be zero for convenience. The steady state solutions of (4) and (13) for the two active layers must then satisfy

$$\phi_2 = -g_2\eta_2, \quad \phi_1 = -g_1\eta_1 - g_2\eta_2, \tag{18}$$

$$J\left(\phi_1, \frac{-\eta_1}{f}\right) = Q_{1,2}, \tag{19}$$

$$J\left(\phi_2, \frac{\eta_1 - \eta_2}{f}\right) = -Q_{1,2}. \tag{20}$$

Summing (19) and (20), using (18), recalling that $J(\psi,\psi) = 0$ for any ψ, and introducing $\beta = \mathrm{d}f/\mathrm{d}y$, one finds that

$$\frac{\beta}{f^2}\frac{\partial}{\partial x}\left(g_1\eta_1^2 + g_2\eta_2^2\right) = 0. \tag{21}$$

Integrating (21) wrt x from the eastern boundary gives the Sverdrup relation

$$g_1\eta_1^2 + g_2\eta_2^2 = g_1\eta_{1E}^2 + g_2\eta_{2E}^2. \tag{22}$$

Using the definition of the Jacobian and (22) one then sees that

$$\begin{aligned} 2g_2\eta_2 J(\eta_2,\eta_1) &= g_2 J\left(\eta_2^2,\eta_1\right) \\ &= -g_1 J\left(\eta_1^2,\eta_1\right) = 0. \end{aligned} \tag{23}$$

Multiplying (19) by η_2, using (18b) to eliminate ϕ_1 and then using (21) and (23) one obtains

$$\beta g_1\eta_1\left(\eta_2 - \eta_1\right)\frac{\partial\eta_1}{\partial x} = -f^2\eta_2 Q_{1,2}. \tag{24}$$

As is well known (e.g. Pedlosky 2012), (22) and (24) together define a first order ordinary differential equation for η_1 which can be solved using elementary methods. This holds even though $Q_{1,2}$ is still an unspecified function of the coordinates x and y.

A remarkably simple expression (see (31) below) for the area integral of $Q_{1,2}$ in region R_1 can be obtained by first integrating (24) wrt x after writing (22) in the form

$$g_2^2\eta_2^2 = g_1g_2\left(a_E^2 - \eta_1^2\right), \tag{25}$$

$$g_1a_E^2 \equiv g_1\eta_{1E}^2 + g_2\eta_{2E}^2. \tag{26}$$

Assuming that the surface heat flux is strong enough to make the upper layer outcrop before it reaches the western boundary and using (25) in (24) one obtains

$$\int_{R_1} f^2 Q_{1,2}\mathrm{d}x = -\beta\int_0^{\eta_{1E}}\left(g_1\eta_1 + \frac{\sqrt{g_1g_2}\,\eta_1^2}{\sqrt{a_E^2 - \eta_1^2}}\right)\mathrm{d}\eta_1. \tag{27}$$

Choosing to define a_E to be negative, allows one to define positive angles ϑ and ϑ_E such that

$$a_E\sin\vartheta \equiv \eta_1, \quad a_E\sin\vartheta_E \equiv \eta_{1E}, \tag{28}$$

and to calculate the second integral on the rhs of (27):

$$\int_{R_1} Q_{1,2}\mathrm{d}x = -\frac{\beta K_{1,2}}{2f^2}, \tag{29}$$

$$K_{1,2} \equiv g_1\eta_{1E}^2 - \sqrt{g_1g_2}\,a_E^2\left(\vartheta_E - \tfrac{1}{2}\sin 2\vartheta_E\right). \tag{30}$$

$K_{1,2}$ only depends on the layer depths along the eastern boundary so is independent of latitude. Consequently (29) can be integrated with respect to latitude:

$$I_Q(1,2) = \int_{R_1} Q_{1,2}\mathrm{d}x\mathrm{d}y = \frac{K_{1,2}}{4\Omega} L(\varphi_2), \qquad (31)$$

$$L(\varphi_2) = -4\Omega \int_{y_2}^{y_P} \frac{\beta}{2f^2}\mathrm{d}y = -\int_{\varphi_2}^{\varphi_P} \frac{\cos\varphi}{R\sin^2\varphi} R\mathrm{d}\varphi, \quad (32)$$

where R is the Earth's radius. In (32), φ_2 is a latitude fractionally poleward of that at which $T_A = T_2$ and φ_P is the most poleward latitude of the eastern boundary. To be more precise, φ_2 is the first latitude at which water in layer 1 is transformed into water in layer 2 sufficiently rapidly for layer 1 to outcrop within the basin. The transition between there being no heat flux and very strong heat fluxes in this model is very sharp because of the formulation of the parameterisation of heat loss in (8) so in this paper the latitude of outcropping will be taken to be the most southerly latitude at which $T_A(x,y) = T_2$.

Expression (31) for the key quantity $I_Q(1,2)$ should be viewed as a dynamical result. The horizontal divergences in the upper and lower layers resulting from the exchange of water between them must be balanced by changes in the potential vorticity of water in the two layers as given by (19) and (20). This determines the east-west slope in the depths of the isopycnals (see (24)) and hence the latitudinal dependence of the zonal integral (29) of the volume flux $Q_{1,2}$.

TABLE 1. Evaluations of $-L(\phi_2)$ defined by (33).

φ°N	$\csc\varphi - 1$
90	0
85	0.0038
80	0.0154
75	0.035
70	0.064
65	0.103
60	0.154
55	0.221
50	0.305

The integral in (32) is easily calculated:

$$L(\varphi_2) = [\csc\varphi]_{\varphi_2}^{\varphi_P} \approx -(\csc\varphi_2 - 1). \qquad (33)$$

Table 1 provides evaluations of $\csc\varphi - 1$ as a function of latitude from which it is clear that the approximation in (33) is accurate to within 10% for evaluations of L with $\varphi = 60^\circ$N in basins where the eastern boundary extends poleward of 80°N .

b. Solutions in the lower layers of a 3-layer model

Consider now the solution for a 3-layer model in region R_2 in figure 3. At the eastern edge of this region, i.e. at the boudary B_1 between regions R_1 and R_2, $\eta_{1B_1} = 0$ and, from (17), $\phi_3 = 0$. Using these points with (22) gives

$$g_2\eta_{2B_1}^2 = g_1\eta_{1E}^2 + g_2\eta_{2E}^2, \quad \phi_{3B_1} = 0. \qquad (34)$$

Within region R_2 itself the steady state solutions of (4) and (13) for the two remaining layers must satisfy

$$\phi_2 = \phi_3 - g_2\eta_2, \qquad (35)$$

$$J\left(\phi_2, \frac{-\eta_2}{f}\right) = Q_{2,3}, \qquad (36)$$

$$J\left(\phi_3, \frac{H+\eta_2}{f}\right) = -Q_{2,3}. \qquad (37)$$

Summing (36) and (37), assuming that the bathymetry is flat, and integrating wrt x westward from B_1, (i.e. repeating the steps in the derivation of (22)) one obtains the Sverdrup relation for region R_2 in the form:

$$g_2\eta_2^2 + 2H\phi_3 = g_2\eta_{2B_1}^2 + 2H\phi_{3B_1}. \qquad (38)$$

Combining (38) and (34) then gives

$$g_2\eta_2^2 + 2H\phi_3 = g_1\eta_{1E}^2 + g_2\eta_{2E}^2. \qquad (39)$$

(39) implies that $J(\eta_2, \phi_3) = 0$ and by similar steps to those in the derivation of (24) one finds that

$$\beta g_2\eta_2(H+\eta_2)\frac{\partial\eta_2}{\partial x} = -f^2 H Q_{2,3}. \qquad (40)$$

Integrating wrt x and then wrt y as in the derivation of (31) and assuming that the surface heat fluxes in region R_2 poleward of latitude φ_3 are strong enough to make layer 2 outcrop one then finds that

$$I_Q(2,3) = \frac{M_{2,3}}{4\Omega} L(\varphi_3), \qquad (41)$$

$$M_{2,3} \equiv g_2\eta_{2B_1}^2\left(1 + \frac{2\eta_{2B_1}}{3H}\right). \qquad (42)$$

TABLE 2. Evaluations of terms in (31) and (41) using (30) and (42) for selected values of η_{1E} and η_{2E}. Other values used are $g_1 = 2g_2 = 0.008\mathrm{ms}^{-2}$, $H = 4000$m

$-\eta_{1E}$(m)	$-\eta_{2E}$(m)	$\frac{K_{1,2}}{4\Omega}$ (Sv)	$\frac{M_{2,3}}{4\Omega}$ (Sv)
500	1000	4.96	17.1
1000	2000	19.8	50.7
1500	3000	44.6	74.8

Table 2 presents evaluations of the latitude independent factors in (31) that contribute to $I_Q(1,2)$ and those in (41) that contribute to $I_Q(2,3)$ for a three-layer model whose layer temperatures are 10°C, 4°C and −2°C and whose salinity is 35 ppt in all layers.

In order to combine tables 1 and 2 it is necessary to specify the lowest latitudes at which the transformations from 10°C to 4°C water and from 4°C to −2°C water take place. The surface air temperature in the North Atlantic is colder on the western side of the basin so the latitudes should be based on the air temperatures there. The surface air temperature east of the Grand Banks (at 50°N) varies from 0°C in February to 10°C in July, so the steady-state calculation that has been posed is clearly an over-simplification. Given this position a reasonable approach is to specify some plausible values for these latitudes and to interpret the results with caution. It will be assumed in this and later calculations that 4°C water will start to form at 60°N and −2°C water at 70°N, noting that a more southerly latitude of 50°N could plausibly be used for the formation of 4°C water and that this would double the amount of water transformed.

With the above choices taking the depths of the layer interfaces on the eastern boundary to be 1000m and 2000m, one sees from tables 1 and 2 that the diapycnal mass transport from layer 1 to 2, $I_Q(1,2)$, would be $0.154 \times 19.8\text{Sv} = 3.0\text{Sv}$ whilst that from layer 2 to 3 would be $0.064 \times 50.7\text{Sv} = 3.2\text{Sv}$. Clearly the transports in this model depend strongly on the depths of the interfaces on the eastern boundary and the most equatorward latitude at which surface cooling starts to generate water for each of the layers.

The zonal scale of the solutions of (24) and (40) varies with latitude in proportional to βf^{-2}. At high latitudes this scale becomes very small and the surface cooling is likely to become concentrated near the eastern boundary and to give rise to a baroclinic eastern boundary current. This current might be interpreted in the Atlantic as the Norwegian Coastal Current (LaCasce 2004). The typical shapes of the isopycnal gradients in these currents are illustrated in Bell (2011).

c. Solutions in models with more layers

Using proof by induction one can derive similar solutions for models with more layers. These solutions are not used subsequently so are simply stated here; the proof follows the steps already described

In a model with more than $n+1$ layers in the region R_n defined in Figure 3, where the wind stresses are negligible and the ocean is losing heat to the atmosphere, the solution satisfies

$$g_n \eta_n^2 + g_{n+1} \eta_{n+1}^2 = W(n+1), \tag{43}$$

$$\beta g_n \eta_n (\eta_{n+1} - \eta_n) \frac{\partial \eta_n}{\partial x} = -f^2 \eta_{n+1} Q_{n,n+1}, \tag{44}$$

where

$$W(n) \equiv \sum_{i=1}^{n} g_i \eta_{iE}^2 \tag{45}$$

and on the eastern boundary of region n (i.e. on B_{n-1})

$$g_n \eta_n^2 \big|_{B_{n-1}} = W(n), \quad \eta_{n+1}\big|_{B_{n-1}} = \eta_{n+1E}. \tag{46}$$

Repeating the steps in the derivation of (31) one finds that

$$I_Q(n,n+1) = \int_{R_n} Q_{n,n+1} \mathrm{d}x\mathrm{d}y = \frac{K_{n,n+1}}{4\Omega} L(\varphi_{n+1}), \tag{47}$$

$$K_{n,n+1} \equiv W(n) - \sqrt{\frac{g_{n+1}}{g_n}} \left(\vartheta_n - \tfrac{1}{2}\sin 2\vartheta_n\right) W(n+1), \tag{48}$$

$$\sin^2 \vartheta_n \equiv \frac{W(n)}{W(n+1)}. \tag{49}$$

The above derivation has again assumed that the surface heat flux is strong enough that poleward of the most southerly latitude at which $T_A = T_{n+1}$ the nth layer will outcrop. It also requires that the nth layer does not become deeper than the $n+1$th layer at any point in the domain. This can readily be checked using (46a) which with (45) gives a simple expression for the maximum depth reached by the base of the nth layer. For example denoting the ratio of g_1 and g_2 by μ_g (i.e. $\mu_g \equiv g_1/g_2$) and the ratio of η_{1E} and η_{2E} by μ_h (i.e. $\mu_h \equiv \eta_{1E}/\eta_{2E}$) the maximum depth reached by the base of the second layer is $\sqrt{(1+\mu_g \mu_h^2)}$ times its depth at the eastern boundary. With $\mu_g = 2$ and $\mu_h = \frac{1}{2}$ this gives a maximum depth of about $-1.22 \times \eta_{2E}$.

4. Solutions for Ekman driven upwelling

B15 presents numerical solutions obtained using the 3-layer PGEs for sub-polar gyre circulations in wide basins driven by strong Ekman upwelling centred at 55°S. The conceptual summary of the results for a 2-layer model is presented in Figure 4. A sub-polar gyre is obtained between the latitude to the north where the zonal wind stress is a maximum and that to the south where it is a minimum. The range in the wind stress will be denoted by $\tau_{\text{range}} \equiv \tau_{\max} - \tau_{\min}$. The upper layer shoals along the curve shown which lies within the latitudes of maximum and minimum wind stress. The eastern edge of this curve lies at x_1 which is given by

$$2f^2 C(x_1 - x_E) = -\beta g_1 \eta_{1E}^2 \tag{50}$$

Within the region where the upper layer shoals, if the water in the surface layer is colder than the atmosphere (i.e. $T_1 < T_A$), the rate of transformation of water from layer 2 to layer 1, i.e. $Q_{1,2}$, is found to be controlled by the Ekman pumping, C defined in (15), with $Q_{1,2} \approx C$. An approximate expression for the area integral of the rate at which

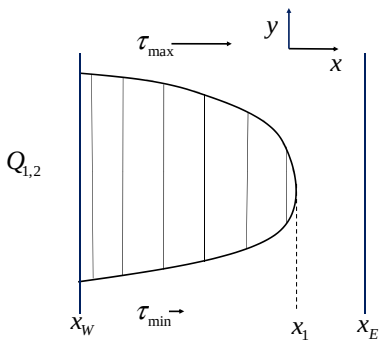

FIG. 4. The conceptual picture used to summarise the numerical results for a 2-layer model. It shows the outcropping region obtained in the sub-polar gyre inside which the net surface heat flux is controlled by the wind stress curl, C.

layer 1 obtains water (a flux with units of $\mathrm{m^3 s^{-1}}$) is then given by

$$I_O = \int\int_{SH} Q_{1,2}\mathrm{d}x\mathrm{d}y \approx C\,(x_1 - x_W)\,\Delta y, \qquad (51)$$

where Δy is the north-south extent of the outcropping region.

Away from the equator to a good approximation $f\rho_0 C = -\partial\tau_x/\partial y$ so one can write

$$f\rho_0 C\Delta y = -\gamma\tau_{\mathrm{range}} \qquad (52)$$

and expect $1/2 \le \gamma \le 1$. Calculating γ by substituting (52) into (51) and using values of I_O from the numerical solutions confirms that it is appropriate to use this range of values of γ and that $\gamma = 0.9$ is a good choice for solutions in which the shoaling occurs in mid-basin. Combining (50) – (52) gives

$$\begin{aligned} I_O &\approx C\,(x_1 - x_E + x_E - x_W)\,\Delta y \\ &= -\frac{\beta g_1 \eta_{1E}^2}{2f^2}\Delta y - \frac{\gamma\tau_{\mathrm{range}}\,(x_E - x_W)}{f\rho_0}. \end{aligned} \qquad (53)$$

Note that the first term on the rhs of (53) is negative whilst the second term is positive and equal to γ times the integral across the basin of the difference between the northward Ekman transports ($\tau/(\rho_0 f)$) where the wind stress is a maximum and a minimum.

5. A 2-layer model of the MOC

Following Walin (1982), Szoeke (1995) and Gnanadesikan (1999) consider the implications of requiring the volume transferred from the upper to the lower layer accompanying surface cooling in the NH to equal the volume transferred from the lower to the upper layer accompanying the warming of cold upwelling water in the SH, I_O as given by (53). Adapting (41) and (42) to the 2-layer model, the rate at which volume is lost from layer 1 to 2 in the NH is given by

$$I_L \equiv -\int\int_{R_1} Q_{1,2}\mathrm{d}x\mathrm{d}y = -\frac{M_{1,2}L(\varphi_2)}{4\Omega}, \qquad (54)$$

$$M_{1,2} = g_1\eta_{1E}^2\left(1 + \frac{2\eta_{1E}}{3H}\right) \approx g_1\eta_{1E}^2. \qquad (55)$$

The final approximation above assumes that $h_{1E} \ll H$. This assumption is made here for simplicity. A similar calculation which does not make this approximation is presented in section 8 below.

Equating I_L as given by (54) with I_O as given by (53) one obtains

$$\begin{aligned} \rho_0 g_1 \eta_{1E}^2 \left[L(\varphi_2)\sin\varphi_S - \frac{\Delta y\cot\varphi_S}{R}\right] \\ = 2\gamma\tau_{\mathrm{range}}\,(x_E - x_W)\,, \end{aligned} \qquad (56)$$

where φ_S is a latitude representative of that where water upwells in the SH.

Taking the water in the two layers to have temperatures of 10°C and 4°C, the value for φ_2 will be set to 60°N, as discussed in section 3b. The upwelling region will be taken to be centred at 55°S, so $\varphi_S = 55°\mathrm{S}$, and its width will be taken to be 10°, so that $\Delta y \approx R/6$. One then finds that $L(\varphi_2)\sin\varphi_S = 0.126$ and $\Delta y\cot\varphi_S = -0.117R$ so that the term in square brackets in (56) equals 0.24. Then taking $\gamma = 0.9$, $\tau_{\mathrm{range}} = 0.15\mathrm{Nm^{-2}}$ and $x_E - x_W = 2\times10^7\mathrm{m}$, one finds that $g_1\eta_{1E}^2 = 2.25\times10^4\mathrm{m^3 s^{-1}}$. As $g_1 = 0.008\mathrm{ms^{-2}}$ for the interface between 4°C and 10°C water this gives $h_{1E} \approx 1680\mathrm{m}$. Using (54) and the full expression in (55) for $M_{1,2}$ the overturning circulation is then

$$\begin{aligned} I_L = -\frac{M_{1,2}L(\varphi_2)}{4\Omega} &\approx 1.6\times10^4\,\frac{0.154}{4\times7\times10^{-5}}\,\mathrm{m^3 s^{-1}} \\ &\approx 8.6\times10^6\mathrm{m^3 s^{-1}}. \end{aligned} \qquad (57)$$

This value should be compared with the MOC transport at about 60°N rather than the transport obtained from the RAPID array at 26.5°N which is bolstered by the heat losses in the Gulf Stream at about 40°N.

6. Comparisons with Gnanadesikan (1999)

Gnanadesikan (1999) (G99 hereafter) infers the strength of the overturning circulation in the NH, T_n in his notation, from a calculation of the western boundary current involving the depth of the thermocline, D. The formulae for T_n and I_L as given by (54) involve corresponding terms for g', D and $\beta \approx 2\Omega/R$ in G99's notation and g_1, η_{1E} and Ω in the notation of this paper. This agreement is very welcome because the transport in the western

boundary current needs to match the water mass transformations by the surface fluxes for the circulations to be self consistent. (Appendix A of Fürst and Levermann 2012, discusses a number of alternative scalings for T_n.) There appears to be a quantitative difference between the formulae, with G99's choice for his constant of proportionality C giving T_n a factor of 4 larger than would be calculated using the formulae for I_L and the "standard" choices of parameters in this paper, but two factors may account for this discrepancy. First G99 chooses C by fitting to the MOC from a General Circulation Model. This MOC would include a wider range of water masses than the 4°C to 10°C range considered here. Second as already noted the choice of φ_2 used here may be conservative. Choosing a value of 50°N in place of 60°N would double the strength of the circulation.

G99's argument for the overturning circulation in the SH, T_s in his notation, depends on there being a Southern Ocean channel whereas the expression (53) was derived for a basin. The formulae for T_s and I_O nevertheless have a similar dependence on a zonally integrated Ekman flux. In the case of G99 this is a circumpolar Ekman flux within the Drake passage whereas in this paper it is the difference between the basin-wide Ekman fluxes at the latitudes where the wind stress is a maximum and a minimum. The correction to the Ekman flux depends on the eddy bolus transport in G99, proportional to $A_I D$, A_I being the "Gent-McWilliams" diffusion parameter, whilst in this paper the correction depends on the distance between the eastern edge of the shoaling region and the eastern boundary and is proportional to η_{1E}^2. Gnandesikan *et al* (2003) note that a quadratic dependence on D for the correction can produce a better fit to the SH transports in their coarse resolution ocean model than a linear dependence. G99 also includes a parametrisation of diapycnal upwelling through the low-latitude pycnocline which could easily have been included in (56) but has been omitted.

In summary despite the differences in their derivation and interpretation the models of the MOC given here and in G99 produce results that are remarkably similar.

7. Energetics of the N-layer model

As the energetics of the MOC have had a significant influence on ideas about how it is driven (Vallis 2006; Wunsch and Ferrari 2004; Hughes *et al* 2009; Tailleux 2009), and the energetics of the model described in this paper are very straightforward it is pertinent to describe them. The derivations here stem from sections 5.7 and 6.7 of Gill (1982).

The kinetic energy equation is obtained by taking the scalar product of the horizontal momentum equation (3) with $\rho_0 h_i \mathbf{u}_i$:

$$0 = -\rho_0 h_i \left(u_i \frac{\partial \phi_i}{\partial x} + v_i \frac{\partial \phi_i}{\partial y} \right) + (u_i \tau_{xi} + v_i \tau_{yi}) . \qquad (58)$$

The equation for the evolution of potential energy is obtained by multiplying (5) by $\rho_0 \phi_i$:

$$\rho_0 \phi_i \frac{\partial h_i}{\partial t} + \rho_0 \phi_i \nabla . (h_i \mathbf{u}_i) = \rho_0 \phi_i (Q_{i,i+1} - Q_{i-1,i}) . \qquad (59)$$

As the upper and lower interfaces are stationary, using (2) and (4) the first term on the lhs of (59) when summed over all layers reduces to the familiar form for the rate of change of potential energy:

$$\begin{aligned} \rho_0 \sum_{i=1}^{N} \phi_i \frac{\partial}{\partial t} (-\eta_i + \eta_{i-1}) & \\ = \rho_0 \sum_{i=1}^{N} -\phi_i \frac{\partial \eta_i}{\partial t} + (\phi_{i-1} + g_{i-1} \eta_{i-1}) \frac{\partial \eta_{i-1}}{\partial t} & \qquad (60) \\ = \rho_0 \sum_{i=1}^{N-1} g_i \frac{\partial}{\partial t} \frac{\eta_i^2}{2} . & \end{aligned}$$

When (58) and (59) are added together the first term on the rhs of (58) and the second term on the lhs of (59) can clearly be combined into the divergence of the horizontal flux $\rho_0 \phi_i h_i \mathbf{u}_i$. The final term on the rhs of (58) is then the energy input by the surface wind stress and the term on the rhs of (59) is the potential energy input by the surface buoyancy fluxes. If at a particular point (x, y) the two layers directly affected by the buoyancy flux are layers p and $p+1$ then the total input to the potential energy by the buoyancy flux, $Q_{p,p+1}$, summed over the two layers affected is given by $\rho_0 (\phi_p - \phi_{p+1}) Q_{p,p+1}$. From (4) this is equal to $-\rho_0 g_p \eta_p Q_{p,p+1}$. Hence when the surface heating occurs in shallow layers at the surface and the cooling occurs in deep surface layers (as envisaged in this paper) the buoyancy forcing is a net sink of potential energy.

Two further points should be made before leaving the energetics. Firstly the expressions described above only apply to the ocean interior, not to the boundary current regions where one would expect there to be some additional dissipation of energy. Secondly the energetics only place one constraint on the motions. When this constraint is sufficient to arrest any flow it is of great interest but in situations where it is not its importance diminishes.

8. A three-layer model of the MOC

This section extends the argument of the previous subsection to a 3-layer model. Subsection 8a describes the conceptual summary of the results for a 3-layer model in the SH corresponding to those described in section 4 above. Subsection 8b then defines the model's formulation. It transpires that the solution for η_{2B_1} can be obtained independently from that of h_{1E}, so the solution for η_{2B_1} is presented in subsection 8c and that for h_{1E} in subsection 8d. The derivations of technical details of the solutions are presented in the appendix.

a. 3-layer Ekman upwelling solution in SH

Figure 5 provides a conceptual summary of the results obtained for the case of a 3-layer model similar to that of figure 4 for a 2-layer model. The upper layer shoals

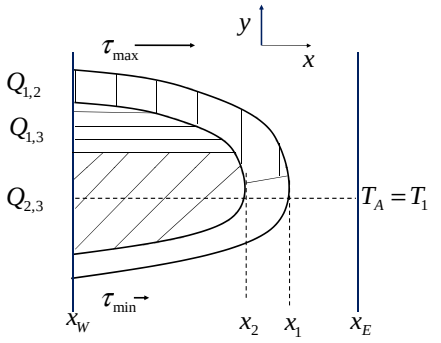

FIG. 5. The conceptual picture used to summarise the numerical results for a 3-layer model. The regions in which $Q_{1,2}$, $Q_{1,3}$ and $Q_{2,3}$ are non-zero are shaded vertically, horizontally and diagonally respectively. The outcrop longitudes x_1 and x_2 are also indicated. For this case a suitable value for δ_1 would be about 0.4.

along the curve whose eastern edge lies at x_1 and the second layer shoals along the curve whose eastern edge is at x_2. x_2 is given by

$$2f^2C(x_2-x_E) = -\beta g_2 \eta_{2B_1}^2, \tag{61}$$

in which η_{2B_1} is defined by (34). (50) can be used to predict x_1 (though alternative expressions are possible).

Where one or both upper layers shoal the rate of water mass transformation is again given to a good approximation by the wind stress curl, C. But depending on the relative temperatures of the upper layers and that of the imposed atmospheric surface, water may be transformed from layer 2 into layer 1, layer 3 into layer 2 or directly from layer 3 into layer 1. Assuming that wherever it shoals layer 2 is cooler than the surface atmosphere, the rate at which water is extracted from layer 3 can be expressed as

$$I_{X3} = \int\int_{SH} (Q_{1,3}+Q_{2,3})\,\mathrm{d}x\mathrm{d}y \approx C(x_2-x_W)\,\Delta y. \tag{62}$$

Using (52) and (61) in (62) one obtains

$$I_{X3} = -\frac{\beta}{2f^2} g_2 \eta_{2B_1}^2 \Delta y - \frac{\gamma \tau_{\text{range}}}{f\rho_0}(x_E - x_W). \tag{63}$$

Similarly the rate at which layer 1 obtains water from other layers can be expressed as

$$I_{O1} = \int\int_{SH} (Q_{1,2}+Q_{1,3})\,\mathrm{d}x\mathrm{d}y \approx C(x_1-x_W)\,\delta_1\Delta y, \tag{64}$$

where δ_1 depends on the fraction of the region where the upper layer shoals which is equatorward of the latitude at which $T_A = T_1$. If the latitudes at which the wind stress curl is a maximum and $T_A = T_1$ coincide then an appropriate value for δ_1 would be somewhat less than $\frac{1}{2}$ because the upper layer can be expected to shoal equatorward of the line where $T_A = T_1$ (see figure 5). Combining (64) with (50) and (52) one obtains

$$I_{O1} = -\frac{\beta}{2f^2} g_1 \eta_{1E}^2 \delta_1 \Delta y - \frac{\delta_1 \gamma}{f\rho_0}\tau_{\text{range}}(x_E - x_W). \tag{65}$$

b. Model Formulation

Expressions for the area integrals in the SH of the rates at which layer 1 obtains water, I_{O1}, and water is extracted from layer 3, I_{X3}, are given by (65) and (63) respectively.

In the NH, the water lost from layer 1, I_{L1}, is given by

$$I_{L1} \equiv -\int\int_{R_1} Q_{1,2}\,\mathrm{d}x\mathrm{d}y = -\frac{K_{1,2}L(\varphi_2)}{4\Omega}, \tag{66}$$

and the water obtained by layer 3, I_{O3}, is given by

$$I_{O3} \equiv -\int\int_{R_2} Q_{2,3}\,\mathrm{d}x\mathrm{d}y = -\frac{M_{2,3}L(\varphi_3)}{4\Omega}. \tag{67}$$

The problem is closed by demanding that

$$I_{O1} = I_{L1}, \tag{68}$$

$$I_{X3} = I_{O3}. \tag{69}$$

It may be helpful to note that I_{O1}, I_{L1}, I_{X3}, I_{O3}, $K_{1,2}$ and $M_{1,2}$ are all positive whilst $L(\varphi_2)$ and $L(\varphi_3)$ are both negative.

c. Solution for η_{2B_1}

Using (67) and (42) one sees that

$$I_{O3} = -g_2\eta_{2B_1}^2\left(1+\frac{2\eta_{2B_1}}{3H}\right)\frac{L(\varphi_3)}{4\Omega}. \tag{70}$$

In order to obtain results in a compact, non-dimensional, form it is useful to introduce a non-dimensional layer depth

$$\hat{\eta}_{2B_1} \equiv \eta_{2B_1}/H. \tag{71}$$

Combining (63), (69) and (70), after some re-arrangement and simplification one obtains

$$\hat{\eta}_{2B_1}^2\left[\left(1+\frac{2\hat{\eta}_{2B_1}}{3}\right)L(\varphi_3)\sin\varphi_S - \frac{\Delta y\cot\varphi_S}{R}\right] = \Pi. \tag{72}$$

where

$$\Pi \equiv \frac{2\gamma}{\rho_0 g_2 H^2}\tau_{\text{range}}(x_E - x_W), \tag{73}$$

is a suitable non-dimensional form for the forcing.

It is shown in the appendix that this cubic polynomial in $\hat{\eta}_{2B_1}$ has at most one solution in the acceptable range $0 < -\hat{\eta}_{2B_1} < 1$ and that there are solutions with $-\hat{\eta}_{2B_1} > 0$ if

$$\left(1 - \frac{\Delta y \cot \varphi_S}{R}\right)^3 > 3\Pi. \tag{74}$$

The appendix also provides an explicit expression for the solution when (74) holds. Using similar parameter values to before ($x_E - x_W = 2 \times 10^7$m, $g_2 = 4 \times 10^{-3}$ms^{-2} for the interface between water of 4°C and −2°C , $\rho_0 = 10^3$kgm^{-3}, $\Delta y = R/6$, and $H = 4 \times 10^3$m) one finds that $\Pi \approx 6 \times \gamma \times \tau_{\text{range}}$ and (74) reduces to the condition

$$\left(1 - \frac{\cot \varphi_S}{6}\right)^3 > 2 \times \gamma \times \tau_{\text{range}}, \tag{75}$$

where τ_{range} is expressed in Nm^{-2}. The maximum value of the rhs is about 0.3 and the lhs is greater than 1 so (74) is met for realistic parameter values.

Table 3 presents the solutions, $\hat{\eta}_{2B_1}$, of (72) for a range of values of Π and φ_3 obtained using $\varphi_S = 55°$S and $\Delta y = R/6$. For the range of values of φ_3 tabulated, when $\Pi \geq 0.16$ there are no solutions with $\hat{\eta}_{2B_1} < 1$, i.e. when $\Pi \geq 0.16$ the depth of the second interface at the eastern edge of region R_2, $-\eta_{2B_1}$, is greater than the assumed ocean depth of 4000m. Although $-\eta_{2B_1}$ increases with φ_3 (the most southerly latitude in the NH at which water in the third layer is first formed) this dependence is relatively weak; η_{2B_1} depends more on Π which is proportional to the strength of the Ekman upwelling integrated across the basin. Table 3 also presents evaluations of (67) for I_{O3}, the MOC volume transport in the lowest layer, using $g_2 = 4 \times 10^{-3}$ms^{-2} and $\Omega = 7 \times 10^{-5}$s^{-1}. I_{O3} is clearly strongly dependent on Π which, using our standard parameters, is about 0.045 if $\gamma = 0.5$ and 0.09 if $\gamma = 1.0$. As already discussed the large amplitude of the seasonal cycle makes it difficult to judge what value is most appropriate for φ_3. Using $\varphi_3 = 70°$N as previously proposed I_{O3} lies between about 2.5Sv and 4.3Sv. Using $\gamma = 0.9$ one obtains $I_{O3} = 4.1$Sv and $\hat{\eta}_{2B_1} = -0.75$ (i.e. $\eta_{2B_1} = -3000$m). In contrast to η_{2B_1}, I_{O3} depends strongly on both φ_3 and Π. I_{O3} varies by about a factor of 30 (from 0.41 to 12) over the range of parameters covered in the table.

The principal relationship obtained in section 5, (56), re-written for η_{2B_1} rather than η_{1E} in the non-dimensional form used in this sub-section, is

$$\hat{\eta}_{2B_1}^2 \left[L(\varphi_3) \sin \varphi_S - \frac{\Delta y \cot \varphi_S}{R}\right] = \Pi. \tag{76}$$

Table 4 presents values of $\hat{\eta}_{2B_1}$ calculated using (76) together with I_{O3} calculated using these values in (70). Comparing these values with those in table 3 one sees that the solutions for $\hat{\eta}_{2B_1}$ and I_{O3} in table 4 are smaller than those in table 3 but that for the smaller values of Π and the larger values of φ_3 they agree particularly well and the general agreement is quite good. Whilst this provides support for the approximation made in deriving (55) it should be noted that the agreement in the values of I_{O3} is much better than that obtained if the second term in brackets in (70) is neglected (as it was in the derivation of (55)). Neglect of that term results in a gross over-estimate of I_{O3}.

TABLE 3. $\hat{\eta}_{2B_1}$ and I_{O3} (Sv) calculated using (72) and (70) respectively as functions of φ_3 and Π as defined by (73). Values for which there are no acceptable solutions are denoted "ns"

$-\hat{\eta}_{2B_1}$	60°N	65°N	70°N	75°N	80°N
0.02	0.30	0.33	0.36	0.38	0.40
0.04	0.44	0.48	0.51	0.54	0.57
0.06	0.55	0.60	0.64	0.67	0.69
0.08	0.65	0.70	0.75	0.78	0.81
0.10	0.74	0.80	0.85	0.88	0.91
0.12	0.83	0.89	0.94	0.97	1.00
0.14	0.92	0.98	ns	ns	ns
I_{O3}	60°N	65°N	70°N	75°N	80°N
0.02	2.6	2.0	1.4	0.87	0.41
0.04	4.8	3.7	2.5	1.5	0.70
0.06	6.8	5.1	3.4	2.0	0.92
0.08	8.5	6.2	4.1	2.4	1.0
0.10	9.9	7.1	4.6	2.6	1.1
0.12	11.	7.6	4.8	2.7	1.2
0.14	12.	7.9	ns	ns	ns

TABLE 4. $\hat{\eta}_{2B_1}$ and I_{O3} calculated using (76) and (70) for the same values of φ_3 and Π as in table 3

$-\hat{\eta}_{2B_1}$	60°N	65°N	70°N	75°N	80°N
0.02	0.29	0.32	0.34	0.37	0.39
0.04	0.41	0.45	0.49	0.52	0.56
0.06	0.49	0.55	0.59	0.64	0.68
0.08	0.57	0.63	0.69	0.74	0.79
0.10	0.64	0.70	0.77	0.83	0.88
0.12	0.70	0.77	0.84	0.91	0.96
0.14	0.76	0.83	0.91	0.98	ns
I_{O3}	60°N	65°N	70°N	75°N	80°N
0.02	2.4	1.9	1.3	0.83	0.40
0.04	4.2	3.3	2.3	1.4	0.69
0.06	5.8	4.5	3.1	1.9	0.89
0.08	7.2	5.4	3.8	2.2	1.0
0.10	8.3	6.2	4.2	2.5	1.1
0.12	9.3	6.8	4.6	2.6	1.2
0.14	10.	7.3	4.8	2.7	ns

d. Solution for h_{1E}

Having obtained a solution for η_{2B_1}, (65) and (66) can be used within (68) to determine $h_{1E} = -\eta_{1E}$. Simplifying

the result as before one obtains

$$K_{1,2}L(\varphi_2)\sin\varphi_S - \frac{\cot\varphi_S}{R} g_1 \eta_{1E}^2 \delta_1 \Delta y = 2\frac{\delta_1 \gamma}{\rho_0}\tau_{\text{range}}(x_E - x_W). \tag{77}$$

Substituting the definition of $K_{1,2}$, (30), into this expression introduces terms involving ϑ_E which is defined by (28b). Using (26) and (34a) in (28) one finds that

$$\sin\vartheta_E = \sqrt{\frac{g_1}{g_2}}\frac{\eta_{1E}}{\eta_{2B_1}}. \tag{78}$$

Eliminating η_{1E} from (77) in favour of ϑ_E and using (30), (77) can be re-arranged into the form

$$L(\varphi_2)\frac{\sin\varphi_S}{\delta_1}\left(\sin^2\vartheta_E - \sqrt{\frac{g_2}{g_1}}\left(\vartheta_E - \tfrac{1}{2}\sin 2\vartheta_E\right)\right) - \frac{\Delta y\cot\varphi_S}{R}\sin^2\vartheta_E = \frac{\Pi}{\hat{\eta}_{2B_1}^2}. \tag{79}$$

The maximum permissible value of ϑ_E, $\vartheta_{E_{\max}}$, is obtained when $\eta_{1E} = \eta_{2E}$. Using (34a) and (78) one sees that

$$\sin^2\vartheta_{E_{\max}} = \frac{g_1}{g_1+g_2}, \qquad \frac{\eta_{1E\max}^2}{\eta_{2B_1}^2} = \frac{g_2}{g_1+g_2}. \tag{80}$$

It is shown in the appendix that the lhs of (79) is monotonic for the values of ϑ_E in the permissible range. This establishes that there is at most one solution for ϑ_E and makes it easy to check whether there is one.

Table 5 presents the solutions of (79) for η_{1E}/η_{2B_1} obtained using three values of η_{2B_1} and a range values of φ_2 and δ_1. The values have been calculated using the same values of φ_S, $\Delta y/R$, g_1 and g_2 as used before and $\varphi_3 = 70°$. No solutions are shown when η_{1E}/η_{2B_1} is greater than the maximum value given by (80b) which in this case is $1/\sqrt{3} = 0.588$. Clearly η_{1E}/η_{2B_1} is relatively insensitive to $\hat{\eta}_{2B_1}$ and varies significantly with φ_2 and δ_1. The lack of sensitivity to $\hat{\eta}_{2B_1}$ can be partly explained by using (72) to re-express the rhs of (79) in a form that is relatively insensitive to $\hat{\eta}_{2B_1}$.

Finally Table 6 presents evaluations of I_{L1} for a range of values of Π and δ_1 and three values of φ_2 again using $\varphi_3 = 70°$N. The range of values for I_{L1}, the volume transport by the MOC in layer 1, in the parameter range covered by the table is very wide; the values range by more than two orders of magnitude from 0.14Sv to 20Sv. Using the value previously proposed for φ_2, namely $\varphi_2 = 60°$N, $\Pi = 0.8$ and $\hat{\eta}_{2B_1} = -0.75$ as in the main calculation of the previous sub-section, and taking $\delta_1 = 0.5$ one sees from table 6 that $I_{L1} \approx 7.0$Sv and from table 5 that $\eta_{1E}/\eta_{2B_1} \approx 0.55$. Using $\eta_{2B_1} = -3000$m this gives $h_{1E} \approx 1650$m.

TABLE 5. η_{1E}/η_{2B_1} calculated using (79) as a function of φ_2 and δ_1 for three values of $-\hat{\eta}_{2B_1}$: (a) 0.1, (b) 0.5 and (c) 0.9

(a)	50°N	60°N	70°N
0.1	0.19	0.27	0.42
0.3	0.33	0.46	ns
0.5	0.43	ns	ns
0.7	0.50	ns	ns
0.9	0.57	ns	ns
(b)	50°N	60°N	70°N
0.1	0.18	0.26	0.39
0.3	0.32	0.44	ns
0.5	0.40	0.55	ns
0.7	0.47	ns	ns
0.9	0.53	ns	ns
(c)	50°N	60°N	70°N
0.1	0.17	0.24	0.37
0.3	0.30	0.41	ns
0.5	0.38	0.51	ns
0.7	0.44	ns	ns
0.9	0.49	ns	ns

In conclusion the solutions for the 3-layer model appear to be quite consistent with those for the 2-layer model. The total MOC transport obtained using the "standard" parameters for the 3-layer model of $7.0 + 4.1 = 11$Sv is reasonably consistent with that of 8.6Sv obtained for the 2-layer model and the dependence of the transports in the two models on the integral of the Ekman pumping across the basin (through Π) and the most southerly latitudes of cold water formation in the NH (φ_2 or φ_3) are also quite consistent.

TABLE 6. Evaluations of I_{L1} (Sv) as a function of values of Π between 0.2 and 1.0 and of δ_1 between 0.1 and 0.9 for three values of φ_2: (a) 50°N, (b) 60°N, (c) 70°N

(a)	0.2	0.4	0.6	0.8	1.0
0.1	0.17	0.66	1.4	2.4	3.6
0.3	0.46	1.8	3.8	6.4	9.6
0.5	0.67	2.6	5.6	9.5	14.
0.7	0.82	3.2	6.9	12.	18.
0.9	0.90	3.5	7.7	13.	20.
(b)	0.2	0.4	0.6	0.8	1.0
0.1	0.16	0.62	1.3	2.3	3.4
0.3	0.38	1.5	3.2	5.4	8.1
0.5	ns	1.8	4.0	7.0	11.
0.7	ns	ns	ns	ns	11.
(c)	0.1	0.3	0.5	0.7	0.9
0.1	0.14	0.53	1.1	1.9	2.9
0.3	ns	ns	ns	ns	4.8

9. Discussion of other configurations

a. MOCs with and without an Antarctic Circumpolar Channel

Since Cox (1989), discussions of the impact of the Southern Ocean on the MOC have studied the combined impact of an open circumpolar channel and strong westerly winds. This sub-section discusses the MOCs that would be obtained when the winds are present in the absence of a circumpolar channel (i.e. if the Drake passage were closed). This is of interest both because paleo evidence shows that the continents have moved considerably and suggest that the channel has been closed in the past (Hill *et al* 2013) and because it suggests a slightly different interpretation of the role of the channel in the present day MOC. The eastern boundary of the Pacific in that case would run from high northern latitudes to high southern latitudes. One would then expect the convective mixing discussed in section 3 to take place in the SH as well as the NH. This means that the Ekman upwelling in the SH would need to return this volume flux from both hemispheres. If one assumes that the convective flux would be the same in the two hemispheres one would calculate the resulting circulations in the 2-layer model by setting the upwelling flux, I_O as given by (51), equal to twice I_L as given by (54). The interface depths on the eastern boundary would then be shallower than in the solution with $I_O = I_L$, so the total volume transfer to the upper layer in the upwelling region would increase but the return volume flux in the NH would decrease. This calculation highlights the role of the circumpolar channel in disconnecting the waters in high southern latitudes from the MOC and the role of the eastern boundary condition in generating the MOCs through maintaining isopycnal depths that are independent of latitude.

Enderton and Marshall (2009) and Ferreira *et al* (2010) have presented results for a number of configurations of aqua-planet coupled climate models with meridional ridges extending from the North pole either to the South pole or to 35°S or 40°S. The surface temperature fields in the full ridge experiments have east-west variations, shown in figure 9 of Enderton and Marshall (2009), that are consistent with the solutions presented in Bell (2015b). It would be interesting to do a more detailed assessment of these simulations using the ideas and solutions presented in this paper.

b. Discussion of a simple two-basin world ocean

Johnson *et al* (2007) have extended the G99 model to include a representation of net evaporation at low latitudes and precipitation at high latitudes and it is natural to ask whether the present analysis could provide any insight into why the cross-equatorial MOC is so much stronger in the Atlantic than the Pacific Ocean.

The sea surface salinity in the North Pacific is about 2 psu less than that in the North Atlantic (Huang 2010, fig 11.5) and the North Pacific has a strong halocline, which is not present in the North Atlantic, with surface salinities more than 1 psu lower than in the water below. Of course it is possible that these differences are a consequence rather than the cause of the reduced MOC in the Pacific but the paragraphs below argue that these salinity differences would reduce the magnitude of convective mixing and hence weaken the MOC in the Pacific, as envisaged in the experiment described in section 6 of Greatbatch and Lu (2003).

For simplicity the following argument considers only the salinity differences arising in the halocline. More specifically suppose that the depths of the isopycnals at the eastern boundaries in the Pacific and the Atlantic are the same and that the salinities in the upper layer in the North Pacific are ΔS psu lower than those in the Atlantic whilst the salinities of all lower layers are the same as those in the Atlantic surface layer.

The parametrisation of the convective overturning in (8) needs to be adjusted so that overturning does not occur until the water in the surface layer at the atmospheric surface temperature is denser than the water in the layer below. The reduction in surface temperature ΔT°C required to compensate for the increase in density due to a salinity increase of ΔS psu across the halocline is given by

$$\rho \alpha_T \Delta T = \alpha_S \Delta S. \tag{81}$$

Using a thermal expansion coefficient $\rho\alpha_T = 0.135\text{kgm}^{-3}\text{K}^{-1}$ appropriate for cooling water from 10°C to 4°C and $\alpha_S = 0.8\text{kgm}^{-3}\text{psu}^{-1}$ gives $\Delta T = 6\Delta S$.

The atmospheric surface temperature at which the upper layer would become convectively unstable in the North Pacific would then be $6\Delta S$°C lower than that in the North Atlantic. This implies that the latitude at which convective mixing of the surface layer with the layer below would commence would be much further north in the Pacific than the Atlantic. Table 1 shows that the total water mass transformed between layers by convective mixing depends very strongly on the latitude at which it commences; the transformation is reduced by a factor of 10 if the latitude is changed from 60°N to 80°N. So the observed salinity difference could weaken the MOC in the Pacific substantively.

Two additional factors could reduce the water mass transformations in the "real world" Pacific. First it does not extend much beyond 60°N. Second it is wide compared with the Atlantic so the upward displacement of the isopycnals by the winds in the sub-tropical gyre is likely to be greater in the Pacific than the Atlantic. At latitudes where the convective mixing is on the western side of the basin this would reduce the amount of water in the upper layer that could be transformed into lower layer waters.

The above arguments assume that the depths of the isopycnals on the eastern boundaries of the Pacific and Atlantic are the same. In general this will not be the case but the following argument shows that it is true to a good approximation for the simple case of a 2-layer ocean in the world illustrated in Figure 1b which has two continents, one ("America") being specified as before and one ("Africa/Asia") extending only to 30°S (which is the latitude of the southern tip of Africa). The argument exploits the facts that the zonal mean zonal wind is approximately zero at 30°S and that the velocity along the coast in the western boundary current is to a very good approximation in geostrophic balance. Integrating the zonal component of (3) for the upper layer across the entire "Pacific" basin at 30°S, the above points imply that the total northward transport (including that in the western boundary layer) by the upper layer in the "Pacific" at 30°S is given by

$$\begin{aligned}\int_W^E h_1 v_1 \mathrm{d}x &= \int_W^E \frac{-\eta_1}{f}\frac{\partial}{\partial x}\left(-g_1\eta_1+\phi_2\right)\mathrm{d}x \\ &= \frac{g_1}{2f}\left(\eta_{1E}^2-\eta_{1W}^2\right)-\int_W^E \frac{\eta_1}{f}\frac{\partial\phi_2}{\partial x}\mathrm{d}x.\end{aligned} \tag{82}$$

This northward transport is equal to the rate of volume lost from the upper layer in the Pacific due to heat loss, I_L, as given by (54) and (55). Taking $|L(\varphi_2)| \le 0.15$ in (55), noting that $f=-\Omega$ at 30°S and using (82) one obtains

$$\begin{aligned}I_L &= -\frac{g_1}{2\Omega}\left(\eta_{1E}^2-\eta_{1W}^2\right)-\int_W^E \frac{\eta_1}{f}\frac{\partial\phi_2}{\partial x}\mathrm{d}x \\ &\le 0.15\frac{g_1\eta_{1E}^2}{4\Omega}.\end{aligned} \tag{83}$$

If the final term on the second line of (83) is negligible, (83) would imply that η_{1W}^2 is within 10% of η_{1E}^2. The magnitude of this final term can be shown to be of order $(h_1/H)I_L$ and hence negligible by considering the northward transport across 30°S in the lower layer into the Pacific. This must satisfy

$$\begin{aligned}-I_L &= \int_W^E h_2 v_2 \mathrm{d}x \\ &= \int_W^E \frac{(\eta_1-\eta_2)}{f}\frac{\partial\phi_2}{\partial x}\mathrm{d}x \approx \frac{H}{f}\Delta\phi_2,\end{aligned} \tag{84}$$

where $\Delta\phi_2$ is representative of east-west differences in ϕ_2. Using this scaling for ϕ_2 in (83) confirms that the last term on the lhs of (83) is of order $(h_1/H)I_L$.

It is then reasonable to take the value of h_{1W} in the Pacific at 30°S to be equal to h_{1E} in the Atlantic. The above argument then implies that the depths of the isopycnals in this simple 2-layer model for a 2-basin world would agree to within 10%.

10. Comparison with previous work

Because of the importance and subtle nature of the MOC the literature on it is very large. Radko and Kamenkovich (2011), Drijfhout *et al* (2013) and Schloesser *et al* (2014) provide good overviews. The discussion below focuses on a fairly small number of papers that are particularly relevant either to this report or to Bell (2015b).

a. The role of Ekman upwelling in the Southern Ocean

Webb and Suginohara (2001) concluded that "a large fraction of the water mass conversion, associated with the upwelling branch of the thermohaline circulation, occurs in the surface layers of the Southern Ocean". This statement was based on analyses of model simulations by Döös and Webb (1994), Toggweiler and Samuels (1995), Toggweiler and Samuels (1998), Hasumi and Suginohara (1999) and Tsujino and Suginohara (1999). The latter study is of particular relevance to this paper and B15 because it describes simulations of an ocean basin straddling the equator which is cooled at the surface in one hemisphere and subject to Ekman upwelling in the other. The authors note that "the Ekman upwelling sucks up a subsurface water to the surface layer to enhance heating through the sea surface ..". Klinger *et al* (2003, 2004) provide further study of similar numerical experiments. All these experiments use simplified Ocean General Circulation Models (OGCMs) and a channel which is only 60° longitude wide whereas the study here is based on semi-analytical methods and a "basin" which spans almost 360° of longitude.

b. Simple models of the MOC with Ekman upwelling in a Southern Ocean channel

Samelson (2009) implemented a single layer reduced-gravity model in a configuration similar to that illustrated in Figure 1 with a simple representation of the ACC that he proposed in Samelson (1999). The wind stress in the model was a maximum within the channel, rather than to the north of the channel, and the depth of the warm water layer was reduced to zero close to the northern edge of the channel. A flux of water into the warm layer at the northern boundary of the channel was specified as the difference between the (northward) Ekman flux and the (southward) eddy transport (as in G99). Diabatic forcing (e.g. high latitude cooling) was represented by relaxing the depth of the warm layer toward a value which was specified as a function of latitude and the circulations within the ocean basin were closed by Stommel-like boundary layers. As noted in Bell (2015b), Samelson drew attention to the critical role of the nearly constant layer depth along the eastern boundary in setting the thermocline structure to the north of the channel.

The study of Radko and Kamenkovich (2011) is a natural analytical extension of Samelson (2009). It uses a time-mean 2.5 layer model and employs different dynamical balances in three regions corresponding to the ACC, the interior of the ocean basins and the western boundary currents. The air-sea density flux is a pre-specified function of latitude. A purely zonal solution is sought in the ACC assuming that the Ekman flux is completely balanced by eddy transports (Johnson and Bryden 1989) parametrised as a diffusive flux as in the Gent *et al* (1995) scheme. This determines the depths of the isopycnals on the eastern boundary in terms of the eddy diffusivity K and the strength of the MOC. Solutions are calculated first taking the MOC strength to be pre-specified and later taking it to be proportional to the depth of the upper layer on the eastern boundary as in G99. The wind stress in the SH is taken to be a maximum in the middle of the Drake passage channel and the gyre solutions are calculated using the methods of Rhines and Young (1982).

Nikurashin and Vallis (2011) and Nikurashin and Vallis (2012) develop an attractive zonal-mean representation of the MOC, again for a configuration similar to Figure 1, using the Transformed Eulerian Mean (TEM) formulation for the residual flow inside a flat bottom Drake passage channel. The eddy momentum flux is again parametrised following the ideas of Gent *et al* (1995) and the buoyancy field is advected by the residual flow and subjected to diapycnal diffusion. The isopycnals in the basin north of the channel are taken to be independent of latitude (as they would be close to an eastern boundary) up to the latitude where they are affected by convective mixing. The surface buoyancy field is prescribed as a function of latitude and projected downward convectively in the basin to the level of neutral buoyancy. The problem is closed by no normal flow boundary conditions. The maximum of the wind stress is taken to occur at the northern edge of the channel. The mid-depth stratification of the solutions, h, is found to scale according to the equation derived by G99 and these scalings are reproduced in idealised GCM experiments. The model is able to represent both upper (NADW) and lower (AABW) MOC cells and gives a plausible representation of the Ekman driven upwelling in the SH, the buoyancy loss in the south of the channel and the bouyancy gain in the north of the channel.

In summary in all of the above studies the wind stress maximum in the SH is taken to lie at the northern edge of the Drake passage (or southward of that) and the ACC is represented by a purely zonal current. In the present work the wind stress is taken to be a maximum to the north of Drake passage and simple solutions are found by requiring the wind stress to be zero within the latitudes of the Drake passage which results in a zonal current within the Drake passage channel and a sub-polar gyre to the north of the channel. Neither of these two sets of assumptions and their resulting currents provide accurate representations of the Southern Ocean, which could be considered to lie between the two extremes. In view of this it is interesting to note that the G99 cubic polynomial for the strength of the MOC is obtained for both sets of assumptions. The representation of the surface heat fluxes in the models discussed in this subsection is also very limited; none of them attempt to account for the longitudinal distribution of surface fluxes described in Bell (2015b). The confinement of the region of surface warming in the SH to the latitudes of the channel in the above papers is also a limitation, though perhaps not a crucial one.

c. Representations of the ACC

For many years it seems that it was assumed that the strength of the ACC is largely controlled by the local balance in the zonal component of momentum despite the obvious point that by thermal wind balance the net transport through the Drake passage is mainly dependent on the depths of the isopycnals at its northern boundary (the flow at the bottom can be taken to be small because it is blocked when the bathymetry is realistic). Gnandesikan and Hallberg (2000) and Fučkar and Vallis (2007) were perhaps the first authors in recent years to suggest that remote buoyancy forcing as well as the surface winds in the Southern Ocean can have major impacts on the time-mean ACC.

The last section of Stommel (1957) provides a tentative discussion of the ACC which is relevant to the limitations of the representation of the ACC in Bell (2015b). Stommel notes that the minimum depths of the sills in the Drake passage are only about 1000 m and that the ACC has a generally southward component throughout its entire length except at the Drake passage and one or two other locations where it is deflected sharply northward. He then discusses first the barotropic circulation that would be obtained from the Southern Ocean winds were there a barrier connecting Antarctica to South America and second the flow that would be obtained from a ruptured set of barriers which still obstruct the flow at all latitudes. He notes that in the first case the southern gyre transports about 100 Sv but describes the flow through the passage in the second case as "something of a mystery". There is no reason to suppose that the flow in the second case is given by the Sverdrup transport because there is no single eastern boundary which connects the solution together. The Sverdrup relation can be derived without using an eastern boundary but the east-west Sverdrup transport depends on north-south gradients and cannot be derived without specifying that gradient at some longitude (e.g. using a boundary condition).

The Sverdrup balance for the time-mean flow is modified by mesoscale eddies even within basins because, denoting time-averages by an overbar and differences from the time mean by primes, the Sverdrup balance applies to

$\overline{h^2} = \overline{h}^2 + \overline{h'^2}$. Even this modified form of the Sverdrup balance should not be expected to hold across the ACC where it turns sharply north in the latitudes of the Drake passage. But the modified form should hold between longitudes that do not contain such a boundary layer current provided the interaction with the bathymetry is sufficiently weak (a major qualification!). Thus one might expect the presence of an energetic eddy field or non-zero wind stresses and Ekman upwelling within the latitudes of the Drake passage to modify but not to obliterate the Ekman upwelling mechanism discussed in Bell (2015b). The investigations of Hallberg and Gnanadesikan (2006) and Munday *et al* (2013) appear to be consistent with this suggestion. It is worth noting that Munday *et al* (2013) study a very different set of configurations from the ones envisaged in this report. Their world ocean is only 20° wide and their Ekman upwelling is confined to the channel. Their main focus is on the strength of the ACC and the MOCs in their standard experiments are relatively weak (of order 1-2 Sverdrup).

d. Other particularly relevant papers

Veronis (1978) describes a 2-layer model of the world ocean driven by both surface wind stresses and heat fluxes. The mathematical formulation is very similar to that of Luyten and Stommel (1986) (as they acknowledge). For example his equation (2.34) is essentially the same as the characteristic equation (28) in Bell (2015b). (Veronis uses Q in place of G). The argument in section 9b of this report also uses arguments very similar to those of Veronis: he derives a mass transport balance for the region north of a given latitude in a closed basin (his equation (2.2)) and uses the fact that the flow along the coast in a western boundary layer is geostrophic. He side-steps issues with a Southern Ocean channel by using two "broken" barriers in the Southern Ocean which together cover all latitudes (Veronis 1973). The three main differences between his analysis and that presented here are: (1) he pre-specifies the depth of the isopycnals along the eastern boundaries from observations just to the west of the eastern boundary; (2) he uses the observed latitudes of separation of the western boundary current and infers a "minimal" set of surface heat fluxes required for consistency with them rather than specifying surface heat fluxes directly (3) he attempts to represent the whole ocean circulation using two layers; it is undesirable to do this when one is seeking to represent the MOC because the heat flux budget within different layers is of primary importance (Walin 1982). Veronis also has an interesting iterative approach to the calculation of the solution of the characteristic equation.

Schloesser *et al* (2012) and Schloesser *et al* (2014) investigate the dynamics of the downwelling limb of the circulation in the North Atlantic using both a general circulation model and simplied analytical models. Their analysis starts with the phases of the spin-up of the circulation from rest, which was also the starting point for this study (Bell 2011). The downwelling circulation is driven by meridionally varying surface temperatures and the circulation is closed either by diapycnal upwelling or by flows at the southern boundary. Their analytical results are obtained for a 2-layer model with the temperature of the upper layer set equal to the atmospheric surface temperature that entrains/detrains water into/from the lower layer in a manner which differs in detail from but is somewhat similar to that employed in this paper. Using a no normal flow eastern boundary condition Schloesser *et al* (2012) derive an expression for the overturning transport in the down-welling limb of the circulation which is somewhat similar to the expressions derived in section 3.

The northern and western boundary layers in this report are assumed to be entirely "passive". Huang and Flierl (1987), Salmon (1998), Pedlosky and Spall (2005) and Spall and Pedlosky (2008) provide valuable discussions of these boundary layers and some of their subtleties. Pedlosky and Spall (2005) for example present a series of analytical and numerical calculations for 2-layer models on a β-plane examining the structure of the western (and eastern) boundary layers in models which diffuse the layer depths. They find that the western boundary layer has a double structure with vertical mass fluxes (water mass transformations) in the thermal boundary layer equal and opposite to those in the inner viscous boundary layer and equal in magnitude to those in the interior of the basin.

11. Summary

The aim of this report is to use relatively simple solutions for gyre-scale circulations in the NH and SH that are driven by surface wind stresses and/or Haney-type heat fluxes (specified by (8) - 10)) to derive quantitative estimates of the strength of the main MOC in world oceans such as those illustrated in Figure 1. This parametrisation of the heat fluxes has a reasonable physical basis and is significantly different from that used in the other simple models of the MOC discussed in subsection 10b.

Section 3 derives analytical solutions for 2-, 3- and N-layer models of the down-welling branch of the "North Atlantic" that are driven in the NH solely by heat loss to the atmosphere. Simple expressions for the area integrated volume transfer between layers, defined by (16), are obtained for two active layers ((31), in which the terms are given by (30) and (33)), the lowest layer of a 3-layer model ((41) and (42)) and the nth layer of a reduced gravity model with more than $n+1$ layers ((47) and (48)). All these formulae involve the product of a term which depends only on the depths of the layer interfaces on the eastern boundary and a second term which depends primarily on the latitudes at which the atmospheric surface temperature, T_A, first becomes equal to the temperatures of the sub-surface layers. These formulae are valid for any

specification of T_A as a function of latitude and longitude and determine the strength of the downwelling branch of the MOC.

Section 4 summarises the conceptual picture (figure 4) for sub-polar gyres driven by the Ekman upwelling of the SH winds which was derived from numerical integrations in a previous paper (Bell 2015b). The winds drive cold water to the surface on the western side of the basin and largely control the heat extracted from the atmosphere there. Simple quantitative estimates of the rate of transformation of water in terms of northward Ekman transports integrated across the basin and the depths of the isopycnals on the eastern boundary for a 2-layer model are given by (53).

Section 5 derives a simple 2-layer model of the MOC by requiring the water lost from the upper layer in the "North Atlantic" to be equal to the water transformed back into the upper layer in the Ekman upwelling region of the SH. This determines a linear relationship (56) between the range of the Ekman transports in the SH and the square of the interface depth on the eastern boundary. The latter is approximately proportional to the strength of the MOC. Section 6 compares this model of the MOC with that of Gnanadesikan (1999) and shows that they are generally consistent.

Section 7 recalls the relatively transparent energetics of a layered model which make it clear that the circulation draws its energy from the surface wind forcing. Section 8 presents a 3-layer model of the MOC and concludes that its solutions are generally consistent with those of the 2-layer model. Section 9 briefly discusses a world ocean in which an eastern boundary extends from pole to pole and suggests that convective mixing would occur at high latitudes in both hemispheres. Consideration of that case gives a different perspective on the roles of the Southern Ocean channel and the eastern boundary conditions in shaping the MOC. Section 9 also discusses a 2-basin ocean in which one of the basins has a strong halocline like that in the Pacific. It is shown that according to the model presented here a halocline of the observed strength would greatly reduce the MOC in the basin containing it.

Most of the assumptions and simplifications made in this paper were discussed in the final section of Bell (2015b). Three simplifications are however worth highlighting, the first being that only steady state solutions have been considered. More specifically seasonal variations have not been taken into account despite the fact that the atmospheric forcing of the northern hemisphere branch of the overturning will vary greatly with the season and the total overturning cannot be estimated properly using annual average surface atmospheric temperatures. An analysis similar in concept to that of Johnson and Marshall (2002) is required to estimate the annual mean water mass transformation rate. The second simplification is the neglect of wind forcing for the downwelling branch of the circulation. Although this was partially justified through a scaling argument, it was motivated at least in part by the desire to obtain quantitative estimates whose scaling properties could be readily understood. The third simplification is the restriction of the wind stresses to the north of the channel in the SH. Clearly a better representation of the ACC and its interaction with the wind-driven Ekman upwelling circulation than that discussed here is highly desirable.

Acknowledgments. This work was supported by the Joint UK DECC/Defra Met Office Hadley Centre Climate Programme (GA01101). The author is particurlarly grateful to David Ferreira, David Marshall, Geoff Vallis and Andy White for their advice. The presentation of this report also benefited from two anonymous reviewers of Bell (2015a)

APPENDIX

Properties of the three-layer model of the MOC

This appendix establishes some properties of the 3-layer model of the MOC introduced in section 8

In order to determine the number of relevant roots of the cubic equation (72) it is convenient to re-write it using w in place of $-\hat{\eta}_{2B_1}$ in the two alternative forms

$$\begin{aligned} \mathsf{F} &\equiv w^2\left(1-\tfrac{2}{3}w+a_2\right)-a_0=0, \\ \mathsf{G} &\equiv w^3-b_2w^2+b_0=0, \end{aligned} \tag{A1}$$

in which the constant coefficients a_0, a_2, b_0 and b_2 are all positive. Because $b_0>0$, the product of the three roots of (A1b) is negative. (A1b) will have two positive roots if $\mathsf{G}<0$ for any positive value of w. Differentiating (A1a) one obtains

$$d\mathsf{F}/dw = 2w^2\left(1+a_2-w\right). \tag{A2}$$

At the turning point, $w=1+a_2$ and $\mathsf{F}>0$ and $\mathsf{G}<0$ if

$$\tfrac{1}{3}\left(1+a_2\right)^3 > a_0. \tag{A3}$$

Expressing (A3) in terms of the original variables one obtains (74). The turning point has $w=-\hat{\eta}_{2B_1}>1$ so clearly only the smaller of the two positive roots can be a physical solution.

Explicit solutions to (A1b) can be derived using standard formulae or, following a suggestion by A. A. White, by dividing it through by b_0w^3 which gives

$$b_0^{-1}w^{-3}\mathsf{G} = w^{-3}-b_0^{-1}b_2w^{-1}+b_0^{-1}=0. \tag{A4}$$

This reduced cubic equation in w^{-1} can be solved directly using Cardano's method. Its solutions can be written in terms of the roots of

$$\begin{aligned} s^3 &= -\left(2b_0\right)^{-1}+\sqrt{D}, \\ D &\equiv \left(2b_0\right)^{-2}-b_2^3\left(3b_0\right)^{-3}. \end{aligned} \tag{A5}$$

The condition for $D < 0$ obtained using (A5b) may be shown to be equivalent to (A3) by re-expressing the coefficients b_0 and b_2 in terms of a_0 and a_2 using (A1). Let s_1 be a root of (A5a) whose real part is negative (i.e. $Re(s_1) < 0$). Then the solution of interest, w_1, which is the smaller of the positive roots of w, is given by

$$w_1^{-1} = -Re(s_1) + \sqrt{3}|Im(s_1)|. \tag{A6}$$

In order to establish that the lhs of (79) increases monotonically with ϑ_E over its permissible range of values ($0 < \vartheta_E < \vartheta_{E_{\max}}$) it suffices to show that

$$\mathsf{H} \equiv \sin^2\vartheta_E - \sqrt{\frac{g_2}{g_1}}\left(\vartheta_E - \tfrac{1}{2}\sin 2\vartheta_E\right). \tag{A7}$$

increases monotonically with ϑ_E. Differentiating (A7) one sees that

$$\begin{aligned} d\mathsf{H}/d\vartheta_E &= 2\sin\vartheta_E\cos\vartheta_E - \sqrt{\frac{g_2}{g_1}}\,(1-\cos 2\vartheta_E) \\ &= 2\sin\vartheta_E\left(\cos\vartheta_E - \sqrt{\frac{g_2}{g_1}}\sin\vartheta_E\right). \end{aligned} \tag{A8}$$

From (80a) one sees that $\cot^2\vartheta_{E_{max}} = g_2/g_1$. So $d\mathsf{H}/d\vartheta_E > 0$ for $0 < \vartheta_E < \vartheta_{E_{\max}}$ and $d\mathsf{H}/d\vartheta_E = 0$ for $\vartheta_E = \vartheta_{E_{\max}}$. Hence the lhs of (79) increases monotonically with ϑ_E within its permissible range of values.

References

Bell, M. J., 2011: Ocean circulations driven by meridional density gradients. *Geophys. Astrophys. Fluid Dyn.*, **105**, 182–212. doi: 10.1080/03091929.2010.534468.

——, 2015a: Meridional overturning circulations driven by surface wind and buoyancy forcing. *J. Phys. Oceanogr.*, submitted.

——, 2015b: Water mass transformations driven by Ekman upwelling and surface warming in sub-polar gyres. *J. Phys. Oceanogr.*, submitted.

Cox, M. D., 1989: An idealized model of the world ocean. part I: The global scale water masses. *J. Phys. Oceanogr.*, **19**, 1730–1752.

Döös, K., and D. J. Webb, 1994: The Deacon cell and the other meridional ells in the Southern Ocean. *J. Phys. Oceanogr.*, **24**, 429–442.

Drijfhout, S. S., D. P. Marshall, and H. A. Dijkstra, 2013: Conceptual models of the wind-driven and thermohaline circulation. *Ocean Circulation and Climate: A 21st century perspective*, Siedler, G., S. M. Griffies, J. Gould, and J. Church, Eds., Academic Press, 257–282.

Enderton, D., and J. Marshall, 2009: Explorations of the atmosphere-ocean-ice climates on an aquaplanet and their meridional energy transports. *J. Atmos. Sci.*, **66**, 1593–1611.

Ferreira, D., J. Marshall, and J.-M. Campin, 2010: Localization of deep water formation: Role of atmospheric moisture transport and geometrical constraints on ocean circulation. *J. Clim.*, **23**, 1456–1476.

Fučkar, N. S., and G. K. Vallis, 2007: Interhemispheric influence of surface buoyancy conditions on a circumpolar current. *Geophys. Res. Lett.*, **34**, L14605, doi: 10.1029/2007GL030379.

Fürst, J. J., and A. Levermann, 2012: A minimal model for wind- and mixing-driven overturning: threshold behavior for both driving mechanisms. *Clim. Dyn.*, **38**, 239–260, doi: 10.1007/s00382–011–1003–7.

Gent, P. R., J. Willebrand, T. J. McDougall, and J. C. McWilliams, 1995: Parametrizing eddy-induced tracer transports in ocean circulation models. *J. Phys. Oceanogr.*, **25**, 463–47.

Gill, A. E., 1982: *Atmosphere-ocean dynamics*. Academic Press, 662pp.

Gnanadesikan, A., 1999: A simple predictive model of the structure of the oceanic pycnocline. *Science*, **283**, 2077–2081.

Gnandesikan, A., and R. W. Hallberg, 2000: On the relationship of the circumpolar current to southern hemisphere winds in coarse-resolution ocean models. *J. Phys. Oceanog.*, **30**, 2013–2034.

——, R. D. Slater, and B. L. Samuels, 2003: Sensitivity of water mass transformation and heat transports to subgridscale resolution in coarse-resolution ocean models. *Geophys. Res. Lett.*, **30**, 1967, doi:10.1029/2003GL018036.

Greatbatch, R. J., and J. Lu, 2003: Reconciling the Stommel box model with the Stommel–Arons model: a possible role for southern hemisphere wind forcing ? *J. Phys. Oceanogr.*, **33**, 1618–1632.

Hallberg, R., and A. Gnanadesikan, 2006: The role of eddies in determining the structure and response of the wind-driven Southern Hemisphere overturning: Results from the modeling Eddies in the Southern Ocean (MESO) Project . *J. Phys. Oceanog.*, **36**, 2232–2252.

Hasumi, H., and N. Suginohara, 1999: Atlantic deep circulation controlled by heating in the southern ocean. *Geophys. Res. Lett.*, **26, 13**, 1873–1876.

Hill, D. J., A. M. Haywood, P. J. Valdes, J. E. Francis, and D. J. Lunt, 2013: Paleogreographic controls on the onset of the Antarctic Circumpolar Current. *Geophys. Res. Lett.*, **40**, 5199–5204, doi:10.1002/grl.50941,2013.

Huang, R. X., and G. R. Flierl, 1987: Two-layer models for the thermocline and current structure in subtropical/subpolar gyres. *J. Phys. Oceanogr.*, **17**, 872–884.

——, 2010: *Ocean circulation: Wind-driven and thermohaline processes*. Cambridge University Press, 791pp.

Hughes, G. O., A. McHogg, and R. W. Griffiths, 2009: Available potential energy and irreversible mixing in the meridional overturning circulation. *J. Phys. Oceanogr.*, **39**, 3130–3146.

Johnson, G. C., and H. L. Bryden, 1989: On the size of the Antarctic Circumpolar Current. *Deep Sea Res.*, **36**, 39–53.

Johnson, H. L., and D. P. Marshall, 2002: A theory for the surface atlantic response to thermohaline variability. *J. Phys. Oceanogr.*, **32**, 1121–1132.

——, ——, and D. A. J. Sproson, 2007: Reconciling theories of a mechanically driven meridional overturning circulation with thermohaline forcing and multiple equilibria. *Clim. Dyn.*, **29**, 821–836.

Josey, S. A., S. Gulev, and L. Yu, 2013: Exchanges through the ocean surface. *Ocean Circulation and Climate*, Siedler, G., S. M. Griffies, J. Gould, and J. A. Church, Eds., Academic Press, 115–140.

Klinger, B. A., S. Drijfhout, J. Marotzke, and J. R. Scott, 2003: Sensitivity of basinwide meridional overturning to diapycnal diffusion and remote wind forcing in an idealized Atlantic-Southern Ocean geometry. *J. Phys. Oceanogr.*, **33**, 249–266.

——, ——, ——, and ——, 2004: Remote wind-driven overturning in the absence of the drake passage effect. *J. Phys. Oceanogr.*, **34**, 1036–1049.

LaCasce, J. H., 2004: Diffusivity and viscosity dependence in the linear thermocline. *J. Mar. Res.*, **62**, 743–769.

Luyten, J. R., and H. Stommel, 1986: Gyres driven by combined wind and buoyancy flux. *J. Phys. Oceanogr.*, **16**, 1551–1560.

Marshall, J., and K. Speer, 2012: Closure of the Meridional Overturning Circulation through Southern Ocean upwelling. *Nature Geosci.*, **5**, 171–180, doi:10.1038/NGE01391.

Munday, D. R., H. L. Johnson, and D. P. Marshall, 2013: Eddy saturation of equilibrated circumpolar currents. *J. Phys. Oceanogr.*, **43**, 507–532.

Nikurashin, M., and G. Vallis, 2011: A theory of deep stratification and overturning circulation in the ocean. *J. Phys. Oceanogr.*, **41**, 485–502.

——, and ——, 2012: A theory of the interhemispheric meridional overturning circulation and associated stratification. *J. Phys. Oceanogr.*, **42**, 1652–1667.

Pedlosky, J., and M. A. Spall, 2005: Boundary intensification of vertical velocity in a β-plane basin. *J. Phys. Oceanogr.*, **35**, 2487–2500.

——, 2012: Theory of oceanic buoyancy driven flows. *Buoyancy-driven flows*, Chassignet, E. P., C. Cenedese, and J. Verron, Eds., Cambridge University Press, 52–117.

Radko, T., and I. Kamenkovich, 2011: Semi-adiabatic model of the deep stratification and meridional overturning. *J. Phys. Oceanogr.*, **41**, 757–780.

——, and J. Marshall, 2006: The Antarctic Circumpolar Current in three dimensions. *J. Phys. Oceanogr.*, **36**, 651–669.

Rhines, P. B., and W. R. Young, 1982: A theory of the wind-driven circulation. part i: Mid-ocean gyres. *J. Mar. Res.*, **40(Suppl.)**, 559–596.

Rintoul, S. R., C. Hughes, and D. Olbers, 2001: The Antarctic Circumpolar Current system. *Ocean Circulation and Climate, 1st Edition*, Siedler, G., J. Church, and J. Gould, Eds., Academic Press, 271–302.

Salmon, R., 1998: *Lectures on Geophysical Fluid Dynamics*. Oxford University Press, 378pp.

Samelson, R. M., 1999: Geostrophic circulation in a rectangular basin with a circumpolar connection. *J. Phys. Oceanogr.*, **29**, 3175–3184.

——, 2009: A simple dynamical model of the warm-water branch of the middepth meridional overturning cell. *J. Phys. Oceanogr.*, **39**, 1216–1230.

Schloesser, F., R. Furue, J. P. M. Jr, and A. Timmermann, 2012: Dynamics of the Atlantic Meridional Overturning Circulation. Part 1: Buoyancy-forced response. *Progres in Oceanogr.*, **101**, 33–62.

——, ——, J. P. McCreary, and A. Timmermann, 2014: Dynamics of the Atlantic Meridional Overturning Circulation. Part 2: Forcing by winds and buoyancy. *Progres in Oceanogr.*, **120**, 154–176.

Spall, M. A., and J. Pedlosky, 2008: Boundary intensification of vertical velocity in a beta-plane basin. *J. Phys. Oceanogr.*, **35**, 2487–2500.

Stommel, H., 1957: A survey of ocean current theory. *Deep Sea Res.*, **4**, 149–184.

Szoeke, R. A. D., 1995: A model of wind- and buoyancy-driven ocean circulation. *J. Phys. Oceanogr.*, **25**, 918–941. doi: 10.1175/1520–0485(1995)025¡0918:AMOWAB¿2.0.CO;2.

Tailleux, R., 2009: On the energetics of stratified turbulent mixing, irreversible thermodynamics, Boussinesq models, and the ocean heat engine controversy. *J. Fluid Mech.*, **638**, 339–382.

Toggweiler, J. R., and B. Samuels, 1995: Effect of Drake passage on the global thermohaline circulation. *Deep-Sea Res.*, **42A**, 477–500.

——, and ——, 1998: On the ocean's large-scale circulation near the limit of no vertical mixing. *J. Phys. Oceanogr.*, **28**, 1832–1852.

Tsujino, H., and N. Suginohara, 1999: Thermohaline circulation enhance by wind forcing. *J. Phys. Oceanogr.*, **29**, 1506–1516.

Vallis, G. K., 2006: *Atmospheric and oceanic fluid dynamics*. Cambridge University Press, 745pp.

Veronis, G., 1973: Model of world ocean circulation: I. wind driven, two-layer. *J. Mar. Res.*, **31**, 228–288.

——, 1978: Model of world ocean circulation: Iii. thermally and wind driven. *J. Mar. Res.*, **36**, 1–44.

Walin, G., 1982: On the relation between sea-surface heat flow and thermal circulation in the ocean. *Tellus*, **34**, 187–195.

Webb, D. J., and N. Suginohara, 2001: The interior circulation of the ocean. *Ocean Circulation and Climate, 1st Edition*, Siedler, G., J. Church, and J. Gould, Eds., Academic Press, 205–214.

Wunsch, C., and R. Ferrari, 2004: Vertical mixing, energy and the general circulation of the oceans. *Ann. Rev. Fluid Mech.*, **36**, 281–314, doi: 10.1146/annurev.fluid.36.050802.122121.

Met Office
FitzRoy Road, Exeter
Devon EX1 3PB
United Kingdom

Tel (UK): 0370 900 0100 (Int): +44 1392 885680
Fax (UK): 0370 900 5050 (Int): +44 1392 885681
enquiries@metoffice.gov.uk
www.metoffice.gov.uk